UNIVERSITY OF CALIFORNIA,

IRVINE

Photoacoustic Microscopy System with PZT Scanner

THESIS

submitted in partial satisfaction of the requirements

for the degree of

MASTER OF SCIENCE

in Biomedical Engineering

by

Jingyu Liu

Thesis Committee:
Professor Zhongping Chen, Chair
Professor William C. Tang
Assistant Professor Michelle Digman

2016

DEDICATION

To my parents Jun Liu, Yanhua Li and my girlfriend Jiaqi Cheng

for their true love and support

TABLE OF CONTENTS

Page

LIST OF FIGURES

LIST OF TABLES

ACKNOWLEDGEMENTS

I would like to express my deepest gratitude to my advisor Dr. Zhongping Chen for his expert guidance, understanding and encouragement throughout my study and research. Without his incredible patience and timely wisdom, this thesis would not have been possible. In addition, I express my appreciation to Dr. William C. Tang and Dr. Michelle Digman for having served on my committee.

I am grateful to Dr. Zhonglie Piao, who taught me a lot about scanner construction, photoacoustic microscopy and optics.

I would also like to thank Tiancheng Huo, Li Qi, Jiang Zhu, Jiawen Li, Mengke Zhang, Buyun Zhang, Yan Li and other members of the Chen Group for their fruitful discussions and friendship.

Finally, I would like to thank my parents and my girlfriend for their unconditional love and support during my study. I would not have been able to complete this thesis without their continuous love and encouragement.

ABSTRACT OF THE THESIS

Photoacoustic Microscopy System with PZT Scanner

By

Jingyu Liu

Master of Science in Biomedical Engineering

University of California, Irvine, 2016

Professor Zhongping Chen, Chair

Photoacoustic Microscopy (PAM) is a noninvasive imaging method with high acoustic resolution and high optical contrast. It can image deeper tissues than optical microscopy methods, such as multi-photon fluorescence microscopy and optical coherence tomography (OCT). Current scanning mechanism in photoacoustic microscopy is mainly based on positional stage, mirror galvanometer and microelectromechanical system (MEMS). My thesis proposes a novel scanning mechanism using Lead zirconate titanate (PZT), which is one type of piezoelectric ceramics. In my study, the PZT raster scanner is fabricated by mounting a multi-mode optical fiber onto the PZT, which is controlled by a functional generator. When a resonant frequency signal is applied to the PZT, the fiber tip will be vibrated, resulting in a raster scanning light beam in one-dimension. Two-dimensional scanning can be realized by combining another orthogonally mounted PZT. Compared with scanning systems such as the linear stage, mirror galvanometer and MEMS, the PZT scanning system has a faster scanning speed, while preserving satisfactory resolution and a sufficient field-of-view (FOV). In addition, the low cost and compatible configuration of the scanner make it promising for the PAM system to be used in clinical application.

I. Introduction

1. Photoacoustic Microscopy

1.1 Principle and advantages

Photoacoustic Microscopy, based on photoacoustic effect, is a novel and increasingly popular biomedical imaging method. The photoacoustic effect is that when a non-ionizing laser delivers short pulses into biological tissues, part of the energy is absorbed and converted into heat. Therefore, it can lead to the expansion and contraction of the tissues in megahertz frequency (ultrasonic waves) due to the nanosecond pulse duration. Then the ultrasonic waves are detected by one or more ultrasonic transducers, which transfer acoustic signal to electrical signal. Photoacoustic images are produced by processing the electrical signal.

The limitation of optical microscopy has promoted the development of PAM. Optical microscopy has excellent imaging contrast in soft tissue, which relies on sharp optical focusing [1]. However, sharp optical focusing gets weaker when photons travel deeper into tissue because of scattering. Generally, the optical diffusion limit is about 1 mm in tissue [2]. Since the ultrasound scattering is two to three orders weaker than optical scattering in biological tissues [3], ultrasound can provide better contrast in the deeper position. On the other hand, in clinical applications, early stage tumors cannot be detected by conventional ultrasonic imaging methods because of its weak contrast. Therefore, PAM can be used to achieve high contrast and deep tissue imaging at the same time.

1.2 Lateral resolution and axial resolution

The lateral resolution of PAM depends on the wavelength of the laser and the numeric aperture of the objective, given by [4],

$$R_L = 0.51\frac{\lambda_O}{NA_O}, \quad (1)$$

where λ_O is the optical wavelength and NA_O is the numerical aperture of the objective. The constant 0.51 is determined by the full width at half maximum of the optical focal spot.

The axial resolution of the photoacoustic microscopy mainly depends on the bandwidth of the ultrasound given by [4],

$$R_A = 0.88v_A/\Delta f_A, \quad (2)$$

where f_A is the bandwidth of the photoacoustic signal which can be approximated as the bandwidth of the ultrasound transducer.

1.3 Maximum imaging depth

The maximum imaging depth of PAM is determined by the ultrasound attenuation, which is closely related to the optical wavelength and ultrasound frequency [5]. The power of the excitation laser beam can be attenuated by tissue absorption and scattering [2]. Scattering is less related to the wavelength compared with absorption. Hemoglobin and water are two major absorbers in tissue. The absorption varies with the optical wavelength. Thus, we can achieve deeper imaging depth when using appropriate wavelength in the system. As we can see from Figure 1, hemoglobin has the lowest absorption at wavelength of about 700 nm, and water has the lowest absorption at wavelength of about 500 nm. It has also been shown that the maximum imaging depth is proportional to the lateral resolution [6]. For current photoacoustic technology, lateral resolution varies from 220 nm to 560 μm while maximum depth varies from 100 μm to 4 cm [4].

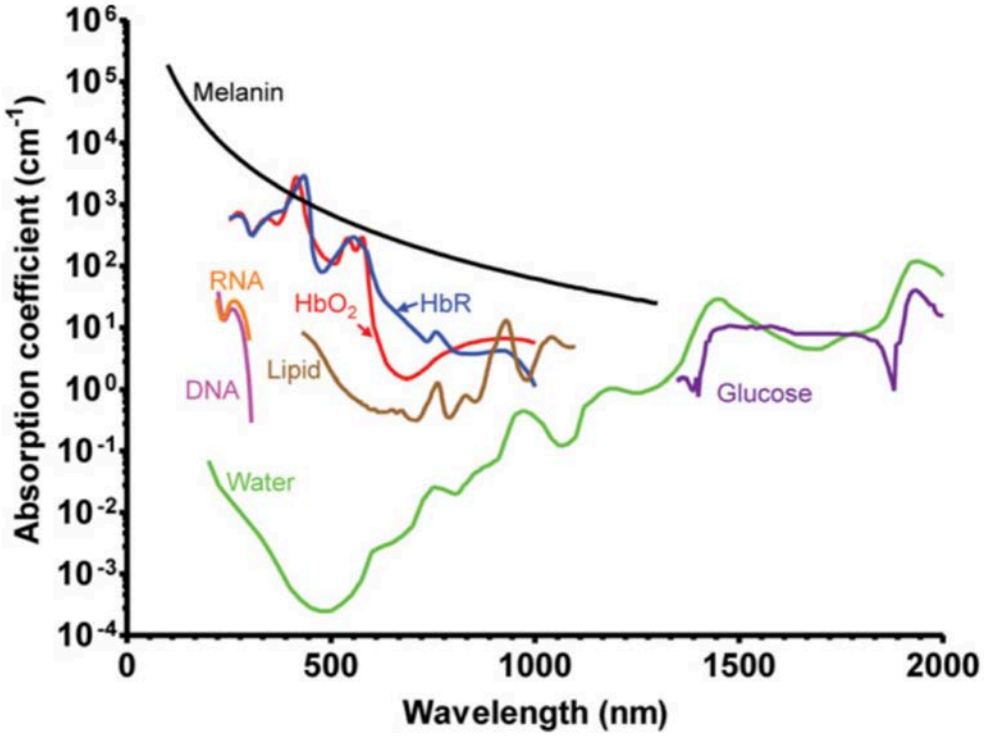

Figure 1 Absorption spectra versus wavelength of several endogenous contrast agents on biological tissue[*]

2. Piezoelectric Ceramics

Piezoelectric Ceramics is a material that can produce an electric charge with mechanical pressure applied on it, and can be physically deformed when an external electric field is applied [7]. So this method can achieve energy conversion between mechanical energy and electricity.

Lead zirconate titanate (PZT) is one type of piezoelectric ceramics. The chemical formula of PZT is Pb $[Zr_xTi_{1-x}]$ O_3 $(0\leq x\leq 1)$ [8]. It is widely used in many places, such as ultrasound transducers and heat sensors, because of its excellent piezoelectricity.

[*] Yao J, Wang L V. Photoacoustic microscopy[J]. Laser & photonics reviews, 2013, 7(5): 758-778.

In my project, PZT is used as the bending actuators to achieve raster scanning. A sinusoidal voltage is applied on the two faces of the PZT, resulting in the sinusoidal bending of PZT. When the sinusoidal signal frequency is equal to the resonant frequency of fiber mounted on the PZT, there will be a large deflection of fiber tip up to several millimeters. Therefore, one-dimensional scanning is achieved. Figure 2 is the PZT used as the scanning actuator. It can be bent because two pieces of PZT are attached to each other. Figure 3 shows the operating principle. This 2-layer element bends when one layer expands while the other contracts. When the fiber is mounted on the PZT, the original PZT resonant frequency changes according to the fiber overhang length. We can change our scanning speed by adjusting the overhang length of fiber.

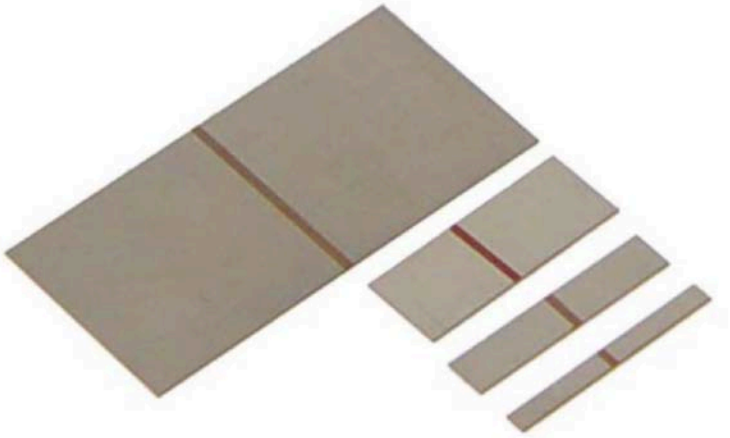

Figure 2 PZT Piezoelectric Ceramics[†]

[†] http://www.piezo.com/prodbm0nav.html

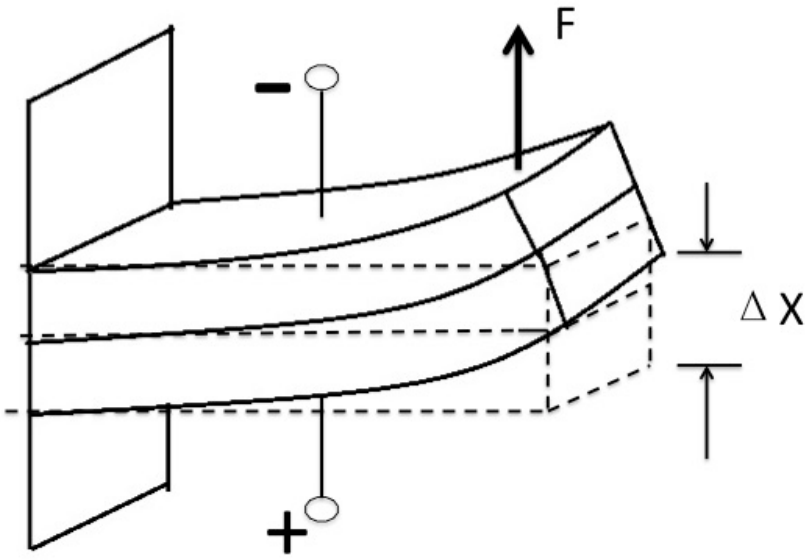

Figure 3 Operating Principle

3. Motivation

In photoacoustic microscopy, galvanometers and MEMS are used to realize different scanning patterns, such as raster scanning or Lissajous scanning. The B-Scan rate can go up to thousands hertz and the scanning range can achieve several millimeters [9]. However, the high price and large size make them hard to be used as portable devices in clinical applications. Instead, the PZT scanner is a good choice for future application in clinical settings. The raster scanning mechanism is realized by resonant/non-resonant fiber mounted on the PZT. So the scanning speed of PZT scanner is depended on the resonant frequency, which is inversely proportional to the overhang length of the fiber. When the overhang length is small enough (less than 9 mm), the B-Scan rate can reach 1 KHz. So we can use a PZT scanning system for fast photoacoustic microscopy imaging.

Moreover, compared with the high price of galvanometers and MEMS, PZT scanning system costs only a few dozen dollars, making it possible for general clinical application of photoacoustic microscopy. Furthermore, in situations that high lateral resolution is not strictly required, such as measuring tissue or blood vessels with hundred micrometers size, we can apply a lens-free system

in the experiment, further cutting the cost of such photoacoustic microscopy systems. The fiber used is THORLAB multimode fiber AFS105/125Y and the core diameter is 105 μm. The maximum lateral resolution of 105 μm in the lens-free system is achieved when the fiber tip is close enough to the sample used in the experiment.

Consequently, fast scanning, low cost and compatible size make it very promising for this type of PAM system to be used in future clinical applications.

II. Photoacoustic Microscopy system with PZT Scanner

1. Scanner

1.1 One-dimensional Scanner

The scanner was fabricated by mounting the fiber on the PZT (PIEZO SYSTEMS, INC. T215-A4SS-503X), and then was placed stably in the middle of a half-inch lens tube. Figure 4 is the prototype one-dimensional scanner, and Figure 5 shows that it was placed in the right middle of a half-inch lens tube, which can be mounted in the imaging system easily.

Figure 4 One-dimensional PZT Scanner

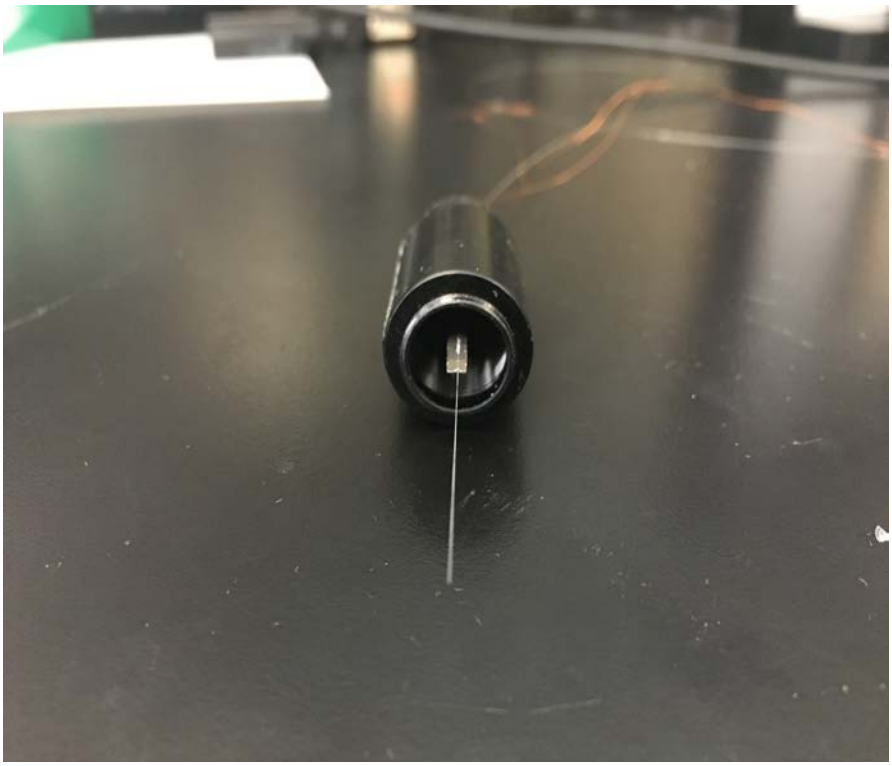

Figure 5 1-D PZT scanner placed in a half-inch tube

The length of the overhang fiber is 32.32 mm. According to the resonant frequency equation [10]:

$$\upsilon = \frac{\beta R}{4\pi L^2}\sqrt{\frac{E}{\rho}},$$

where υ is the resonant frequency, E is the Young's modulus (silica), ρ is the density (silica), L is the fiber overhang length, R is the fiber radius and β is a constant that depends on the boundary condition and vibration mode number, the theoretical resonant frequency was calculated as 95 Hz when the value of β is 3.52. The tested actual resonant frequency is 91 Hz. This frequency deviation is caused by leaving residue glue on the PZT when mounting the fiber, which increased the weight of the PZT. The maximum fiber-tip bending range is 17.34 mm when PZT is driven by the resonant frequency signal. This proves that PZT should be good enough to be used as a raster

scanner. Figure 6 is an image taken when the PZT scanner was scanning. The coin used was a five-cent coin.

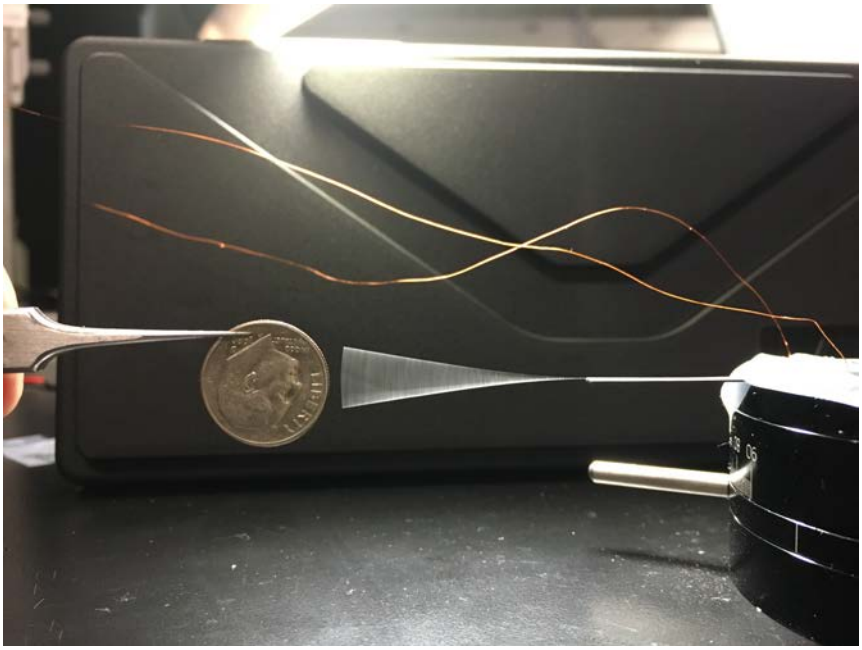

Figure 6 PZT scanner working status

Figure 7 shows that fiber-tip deflection changed with different frequencies. The fiber-tip achieved maximum deflection at the resonant frequency. Fiber deflection was also found at double and triple resonant frequency, which were about 182 Hz and 273 Hz. However, the value of the fiber tip deflection at these two frequences was much lower than that at the resonant frequency. The maximum deflection was 3.03 mm in double resonant frequency and 4.50 mm in triple resonant frequency. It is observed that there were two peak values near triple resonant frequency. One possible reason is that the overhang fiber was too long. It is also found at the triple resonant frequency, not only the tip of the fiber deflected, but the middle part of the overhang fiber was also deflected. Figure 8 shows the relationship between the driving voltages and the fiber-tip deflection.

It is reasonable to conclude that the fiber tip deflection will increase when the driving voltage increases.

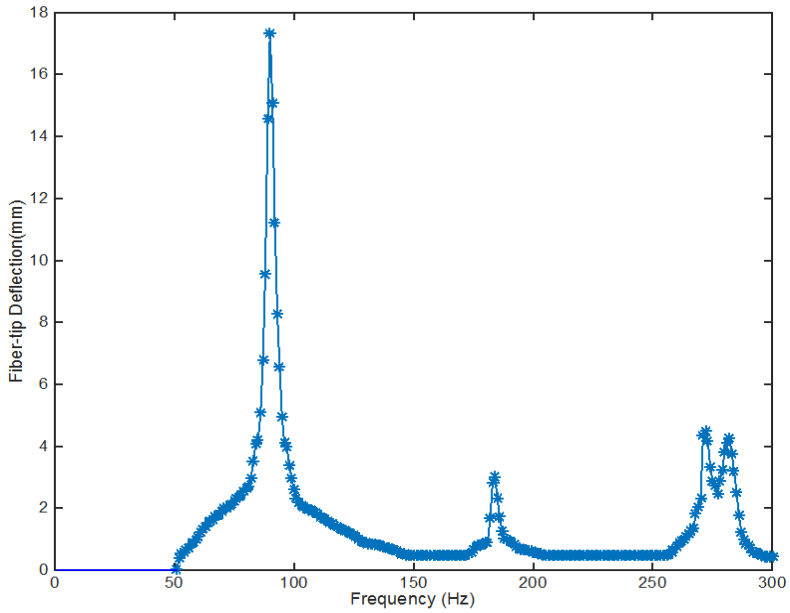

Figure 7 Fiber-tip deflection versus frequency of 1-D PZT scanner

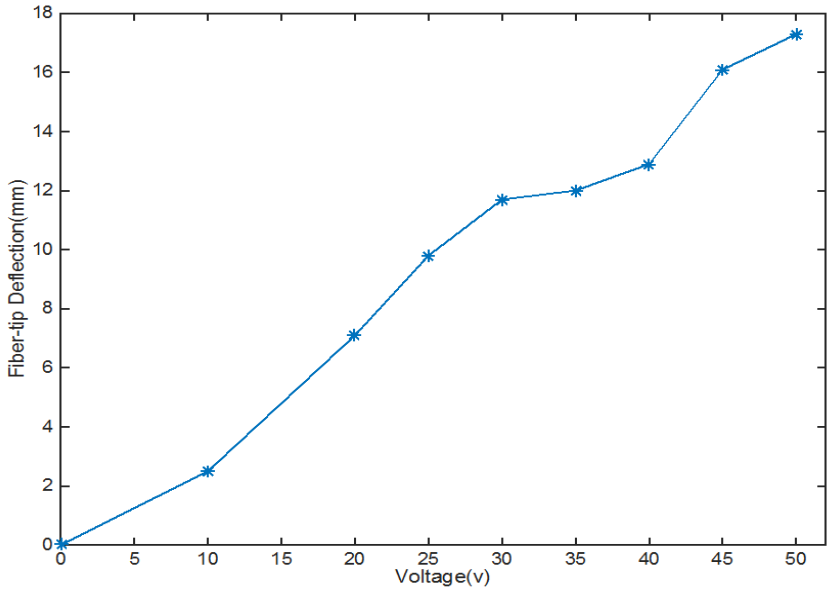

Figure 8 Fiber –tip deflection versus voltage applied on PZT of 1-D PZT scanner

In conclusion, one B-scan image can be obtained by using a one-dimensional scanner. And we can attain a three-dimensional image with the help of a linear stage to scan in another axis.

1.2 Two-dimensional Scanner

The two-dimensional raster scanner was fabricated by mounting another PZT to a one-dimensional scanner, such that the bending axes of the two PZTs were perpendicular to each other. The vertical PZT was stuck vertically on the face of the horizontal PZT. The two-dimensional scanning was achieved by driving the vertical PZT at its resonant frequency while driving the horizontal PZT at its non-resonant frequency. Over ten 2-D PZT scanners were fabricated. It is found that the resonant frequency and the fiber tip deflection were different when the PZT size and overhang fiber length changed. Six well-performed 2-D scanners were selected to be tested, as shown in Figure 9. Their characteristics are listed in Table 1, where HL is the length of PZT in horizontal axis, VL is the length of PZT in the vertical axis, FL is the overhang fiber length, OL is the overlap length of two PZTs, RF is the resonant frequency in the horizontal axis, RD is the fiber tip deflection in the horizontal axis at resonant frequency, and ND is the fiber tip deflection in the vertical axis at non-resonant frequency. All the scanners were driving at the same voltage of 50 V. These scanners were different in the overhang length of the fiber and the way that PZT was stuck. Therefore, their resonant frequency, resonant deflection, and non-resonant deflection were totally different.

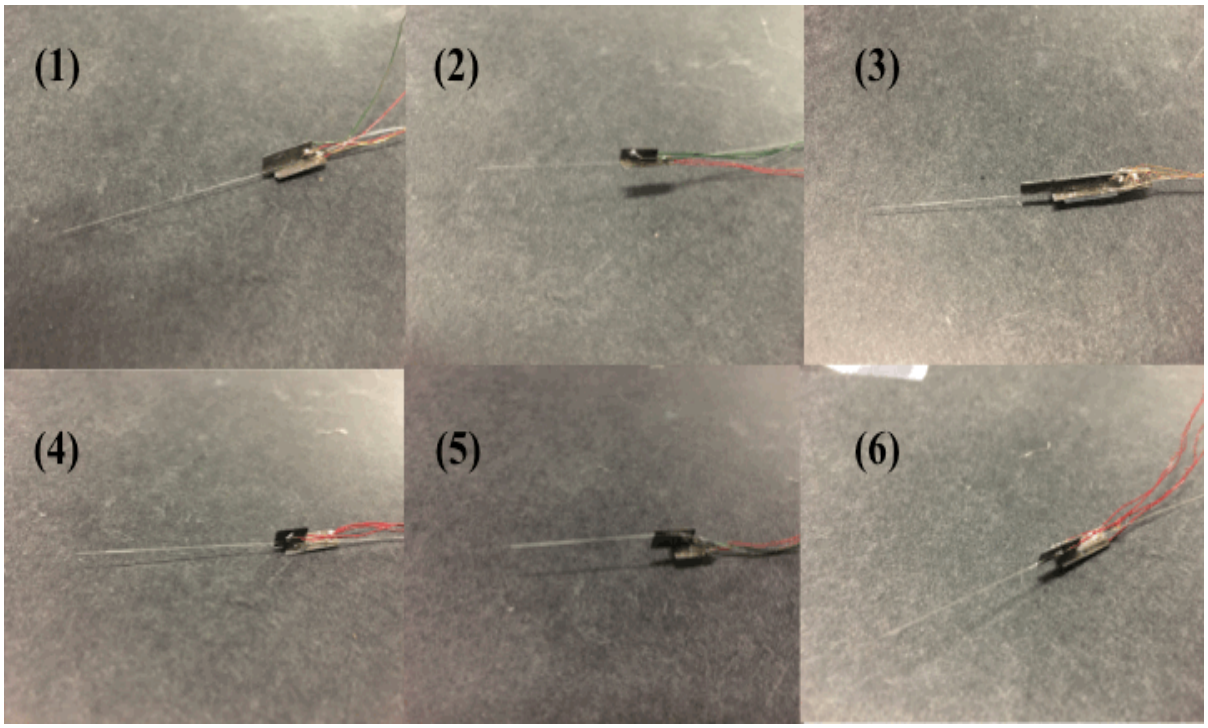

Figure 9 The 2-D PZT Scanners

Table 1 Characteristics of six different 2-D PZT scanners

	HL	VL	FL	OL	RF	RD	ND
1	12.17 mm	12.13 mm	41.45 mm	9.72 mm	53 Hz	1.23 mm	300 μm
2	13.07 mm	9.33 mm	33.66 mm	9.33 mm	61 Hz	0.8 mm	330 μm
3	20.76 mm	21.63 mm	29.23 mm	14.68 mm	93 Hz	1.5 mm	400 μm
4	11.56 mm	6.92 mm	37.44 mm	4.49 mm	48 Hz	1.7 mm	700 μm
5	8.57 mm	9.39 mm	32.51 mm	4.52 mm	68 Hz	2.2 mm	500 μm
6	11.71 mm	9.77 mm	34.27 mm	7.21 mm	66 Hz	2.9 mm	960 μm

According to Table 1, it is found that with a small overlap section, the fiber tip deflection at non-resonant frequency could perform better. Moreover, the size of each PZT cannot determine the final characteristic of the scanner. Also, it is found that the place that the fiber was mounted on

the vertical PZT can influence the fiber tip deflection in the horizontal axis at the resonant frequency. When the mounting position was lower, the fiber would get closer to the horizontal PZT, resulting in a worse resonant fiber tip deflection performance. In Figure 10, the No. 3 scanner has the largest fiber-tip deflection at non-resonant frequency among the three scanners in the left column, for it has the smallest overlap section. Among the three scanners in the right column, the No. 4 scanner has the largest fiber-tip deflection as the result of the best fiber mounted position.

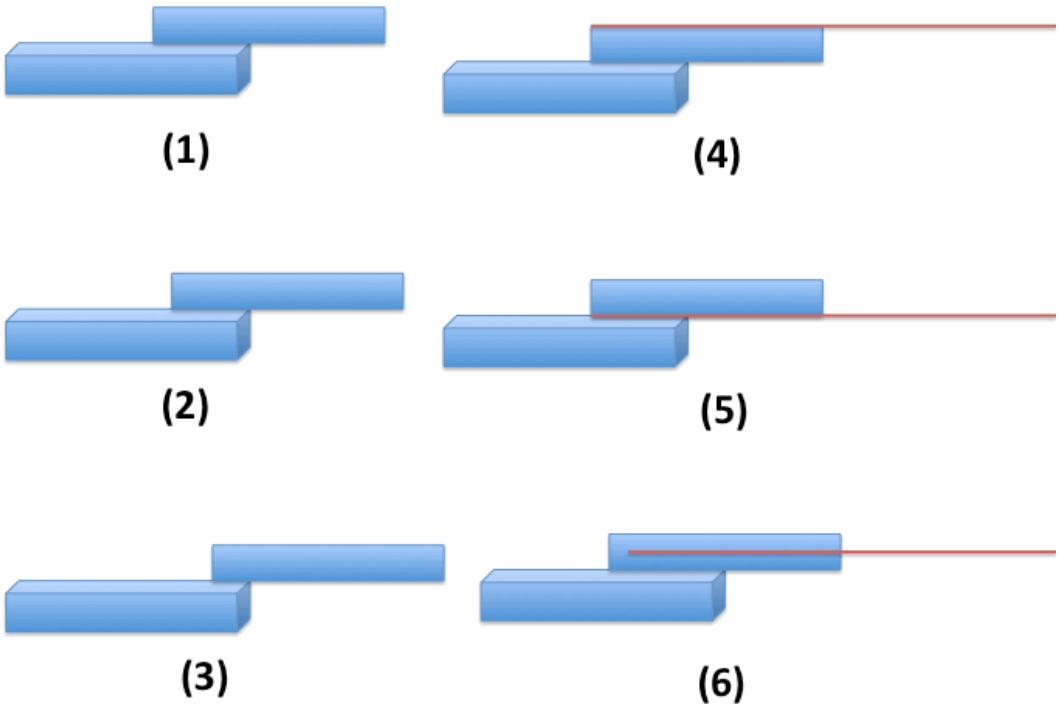

Figure 10 Comparison of different scanners with different overlap section or overhang fiber length

Since both the resonant fiber tip deflection and the non-resonant fiber tip performed well for NO. 6 scanner in Table 1, this scanner was used in the photoacoustic microscopy system.

Using the equation $\upsilon = \frac{\beta R}{4\pi L^2}\sqrt{\frac{E}{\rho}}$, the theoretical resonant frequency was calculated to be 59 Hz, with the measured frequency was 64 Hz. The horizontal PZT affecting the bending of the vertical PZT might cause this deviation. It is recorded that the fiber-tip deflection ranged from 0 Hz to 137 Hz, as shown in Figure 11.

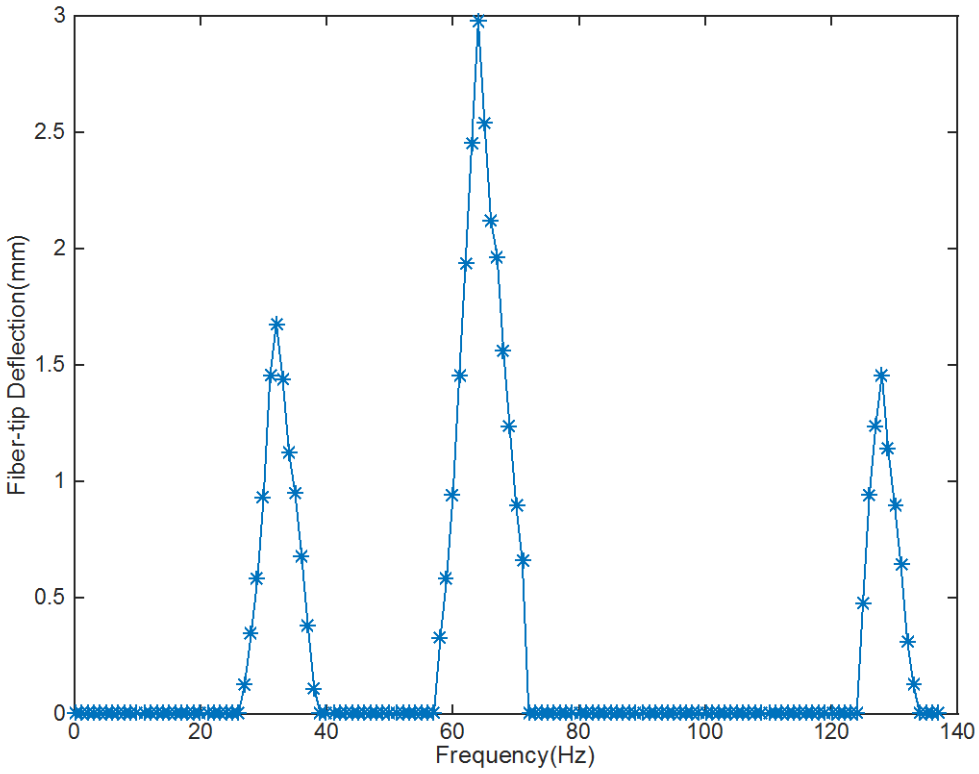

Figure 11 Fiber-tip deflection versus frequency of 2-D PZT scanner

The maximum fiber-tip deflection was at the resonant frequency (64 Hz). And another two significant fiber-tip deflections were also found at half of the resonant frequency and double resonant frequency. This phenomenon was the same as found from 1-D PZT scanner. In addition, Figure 12 shows that the fiber-tip deflection increased with the voltage increasing, from 0 V to 50 V. This phenomenon was also the same as that appeared on 1-D PZT scanner.

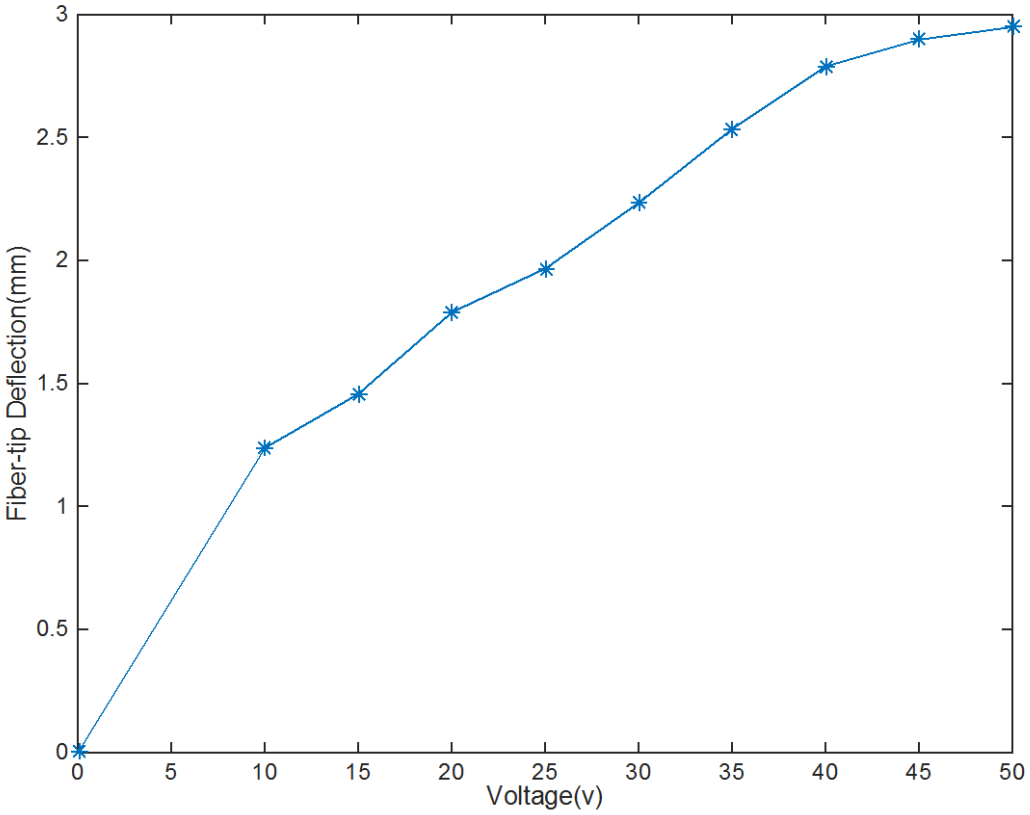

Figure 12 Fiber-tip deflection versus voltage of 2-D PZT scanner

And for the non-resonant fiber-tip deflection, according to the equation [11]:

$$D = 2c(L_1^2 + 2L_1L_2) \times (\frac{V_{applied}}{V_{spec}}),$$

where D is the non-resonant fiber-tip deflection (μm), c is a proportional constant, L_1 is the free length of nonresonant PZT and L_2 is the total length of the resonant PZT and the overhang length of the fiber, it is calculated that the theoretical non-resonant fiber-tip deflection should be 1.1 mm. The actual non-resonant fiber-tip was measured to be about 1 mm. The underperformance may be attributed to the edge effect. Figure 13 shows the 2-D PZT scanner.

Figure 13 The 2-D PZT scanner

2. Photoacoustic Microscopy Imaging System

The photoacoustic microscopy imaging system is composed of a 1654 nm pulse laser (Bright Solutions Srl), pulse receiver, a linear stage, an acoustic transducer (30 MHz), two function generators (Stanford Research Systems Model DS345) and a 3-axis piezo controller (Thorlabs MDT693A). As shown in Figure 14, the laser pulse was coupled into a multi-mode fiber after several optical components. The fiber was mounted on the PZT scanner, and thus, the laser beam can be scanned with the movement of the fiber tip. The objective lens was used to focus the beam onto the target. The ultrasonic signal was received by a 30 MHz transducer and then amplified by the pulse receiver. Finally, the signal was processed in the computer to produce a photoacoustic microscopy image.

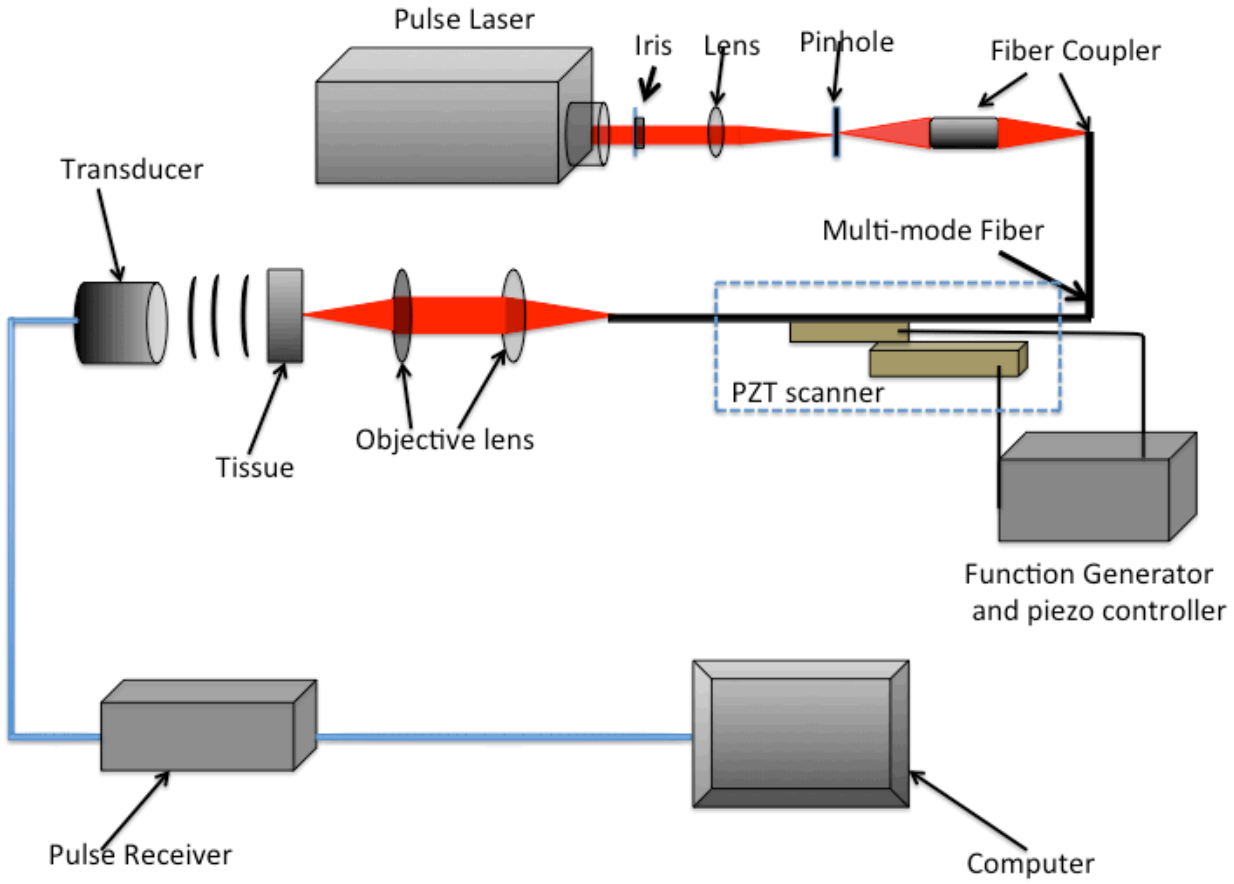

Figure 14 Schematic of PZT-Photoacoustic Microscopic System

3. Experiments

3.1 Resolution test

The USAF 1951 1X resolution target and a DET10C InGaAs Detector were used to measure the lateral resolution of the system. The scanner was placed parallel to the InGaAs Detector, and the resolution target was put between the fiber tip and the InGaAs Detector. The data from the oscilloscope was used to calculate the lateral resolution (Figure 15). The scanner was working at its resonant frequency, and thus, the fiber tip scanned the bars on the resolution target. Therefore, there will be signals of several peaks shown in the oscilloscope, and the peak values were determined by how many bars scanned. The bars with different size were scanned until the peaks in the signal cannot be distinguished, which means that this size of the bar is smaller than the scanner's resolution.

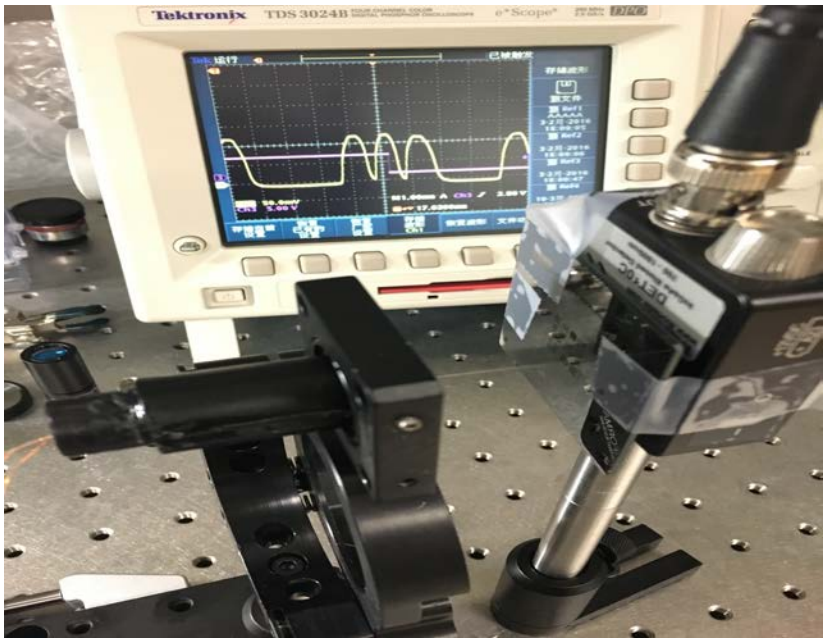

Figure 15 Resolution test

Figure 16 and Figure 17 show the signals when the scanner scanned two kinds of different bars.

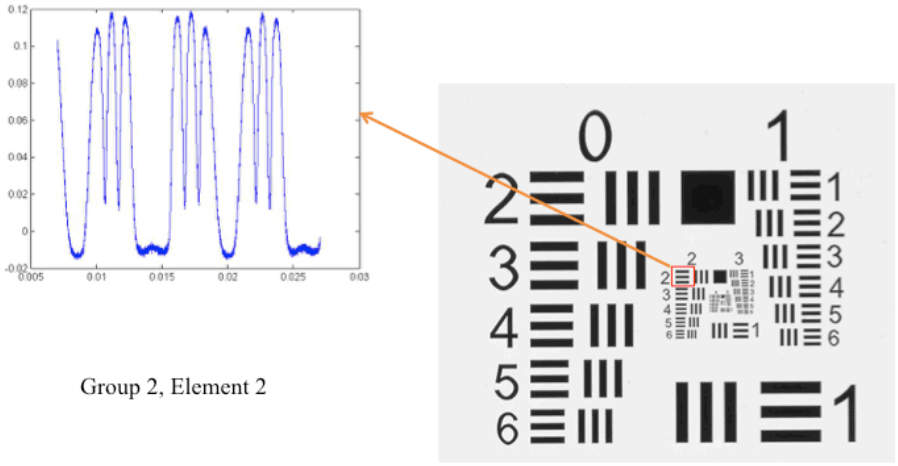

Figure 16 Scanning Group2, Element 2 of resolution target

The element 2 of group 2 was vertically scanned and the signal is shown in Figure 16. The size of each bar is 111.36 μm. Since the peaks can be clearly distinguished, the lateral resolution of the scanner should be smaller than 111.36 μm.

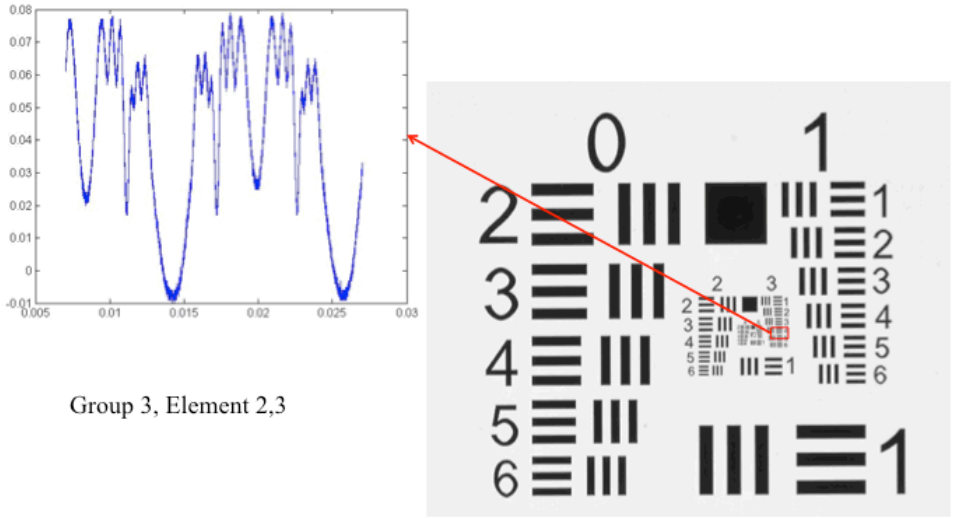

Figure 17 Scanning Group 3, Element 2 and 3 of resolution target

The element 3 and 2 of group 3 were vertically scanned and the signal is shown in Figure 17. The size of a bar in element 3 is 10.08 μm and 8.98 μm in element 2. Since the peaks of element 2 are hard to be distinguished while they can be distinguished in element 3, the lateral resolution of the scanner should be 10.08 μm.

As for the axial resolution, the 30MHz transducer was used, and the axial resolution can be calculated by:

$$R_A = 0.88 v_A / \Delta f_A,$$

where R_A is the axial resolution, v_A is the velocity of sound and Δf_A is the bandwidth of the ultrasound transducer. The theoretical R_A was about 9.97 μm.

3.2 Photoacoustic microscopy imaging using one-dimensional PZT scanner

The one-dimensional PZT scanner was used in the system for photoacoustic microscopy imaging, as shown in Figure 18. The sample was placed between the objective and the transducer. The scanner was mounted on the linear stage. The laser beam from the pulse laser was coupled into the multimode fiber. One functional generator and one 3-axis piezo controller were used to supply voltage to the scanner.

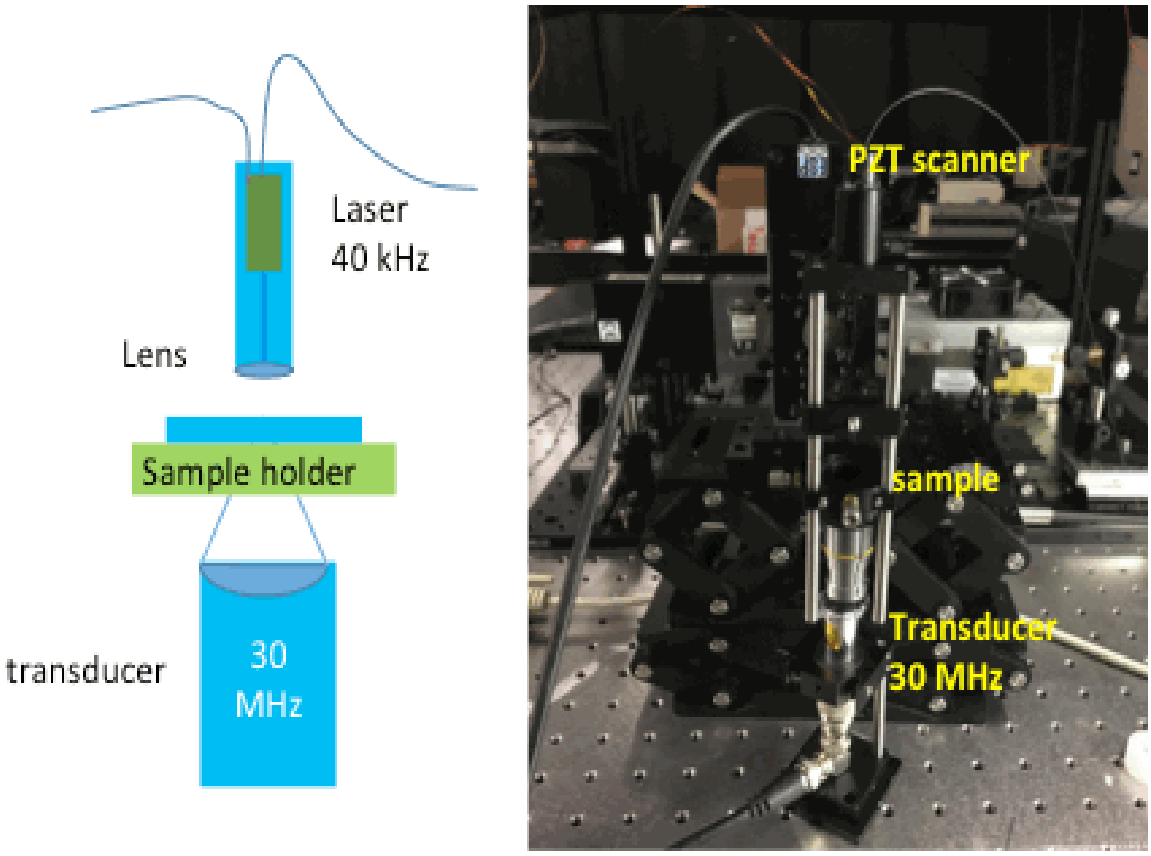

Figure 18 Imaging system

The one-dimensional PZT scanner was working at its resonant frequency and human hairs (~100 μm) were imaged. The scanning speed was 80 Hz. The laser repetition rate was 40 Hz and the pulse energy was 7.5 μJ. Since the PZT scanner only scanned in one dimension, a B-Scan image was obtained (Figure 19). It could be observed that the cross-section of the two hairs was imaged.

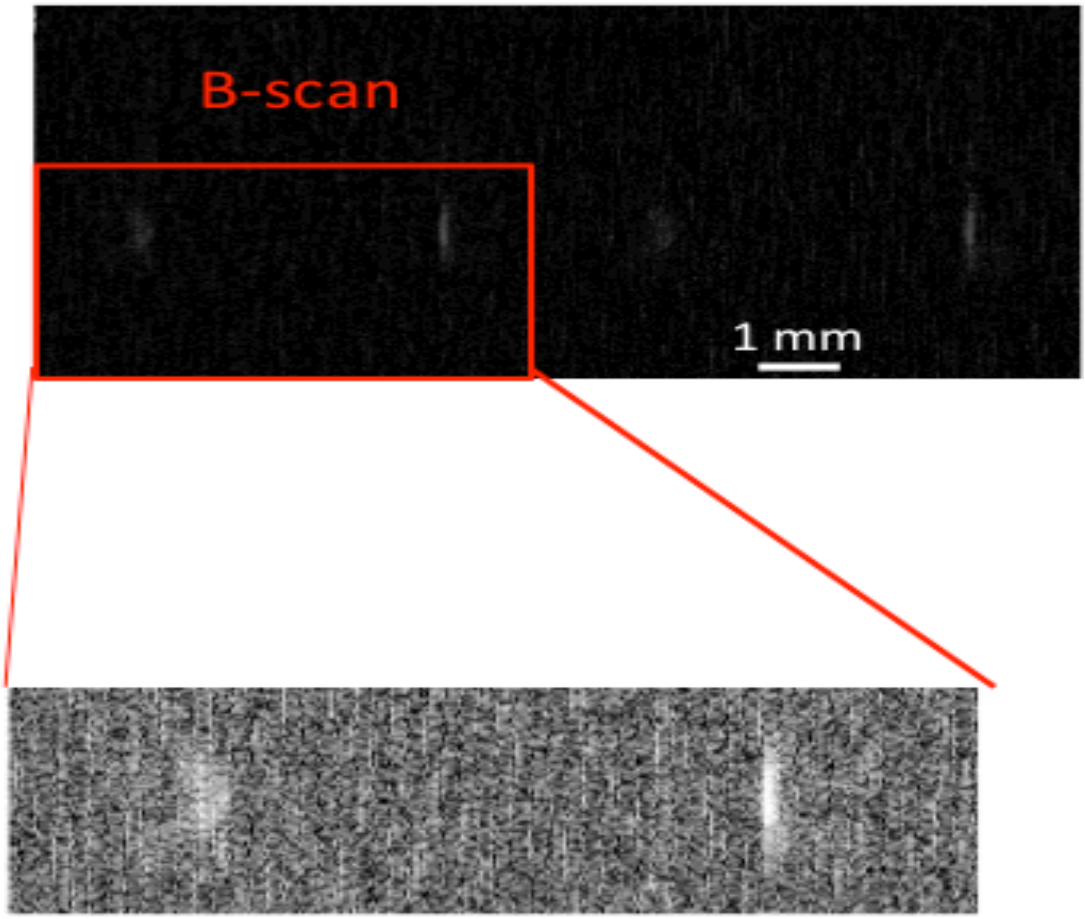

Figure 19 B-scan of human hair

Furthermore, a miniature linear stage (Newport MFN25CC) was used to achieve two-dimensional raster scanning. Carbon fiber was used as a sample. In Figure 20, every B-Scan was acquired by using the 1-D scanner and the C-Scan was achieved by moving the linear stage. The B-scan scanning speed was equal to the 1-D PZT scanner resonant frequency. The C-scan speed was the moving speed of the linear stage. The 1-D PZT scanner and linear stage were used together to achieve 2-D scanning.

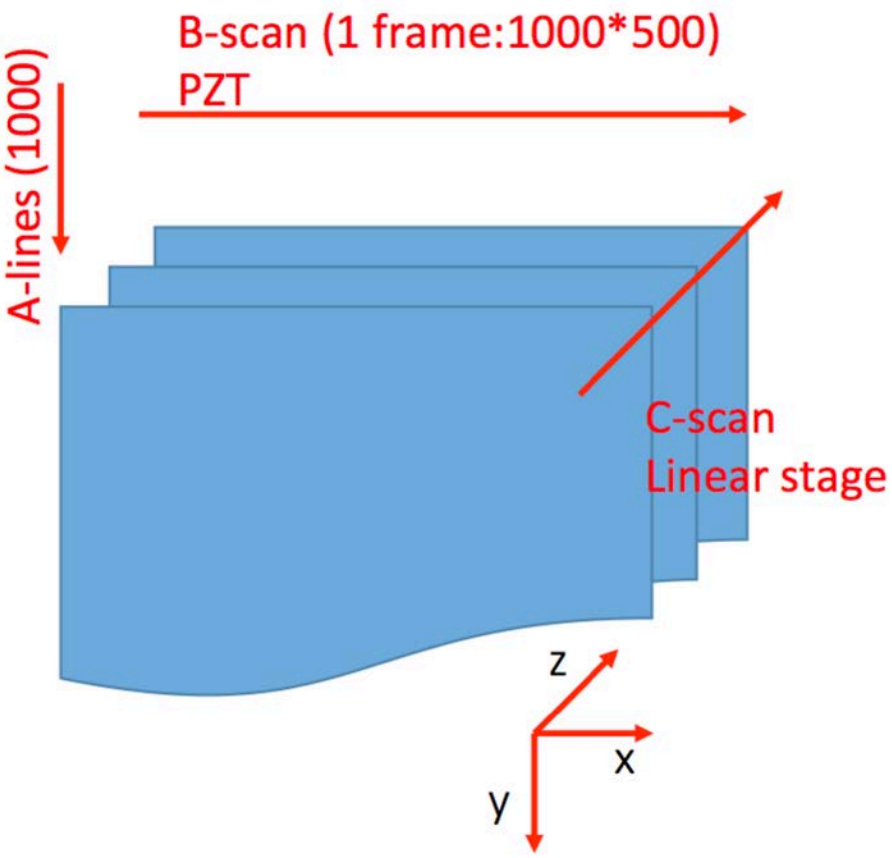

Figure 20 2-D scanning mechanism for 1-D PZT scanner

Figure 21 shows the 2-D image of the carbon fiber network. The scanning speed was 80 Hz. The laser repetition rate was 40 Hz and the pulse energy was 7.5 μJ. The axis x was the 1-D PZT scanner scanning axis and the axis z was the linear stage moving the axis. A 2-D image was finally obtained by using the system.

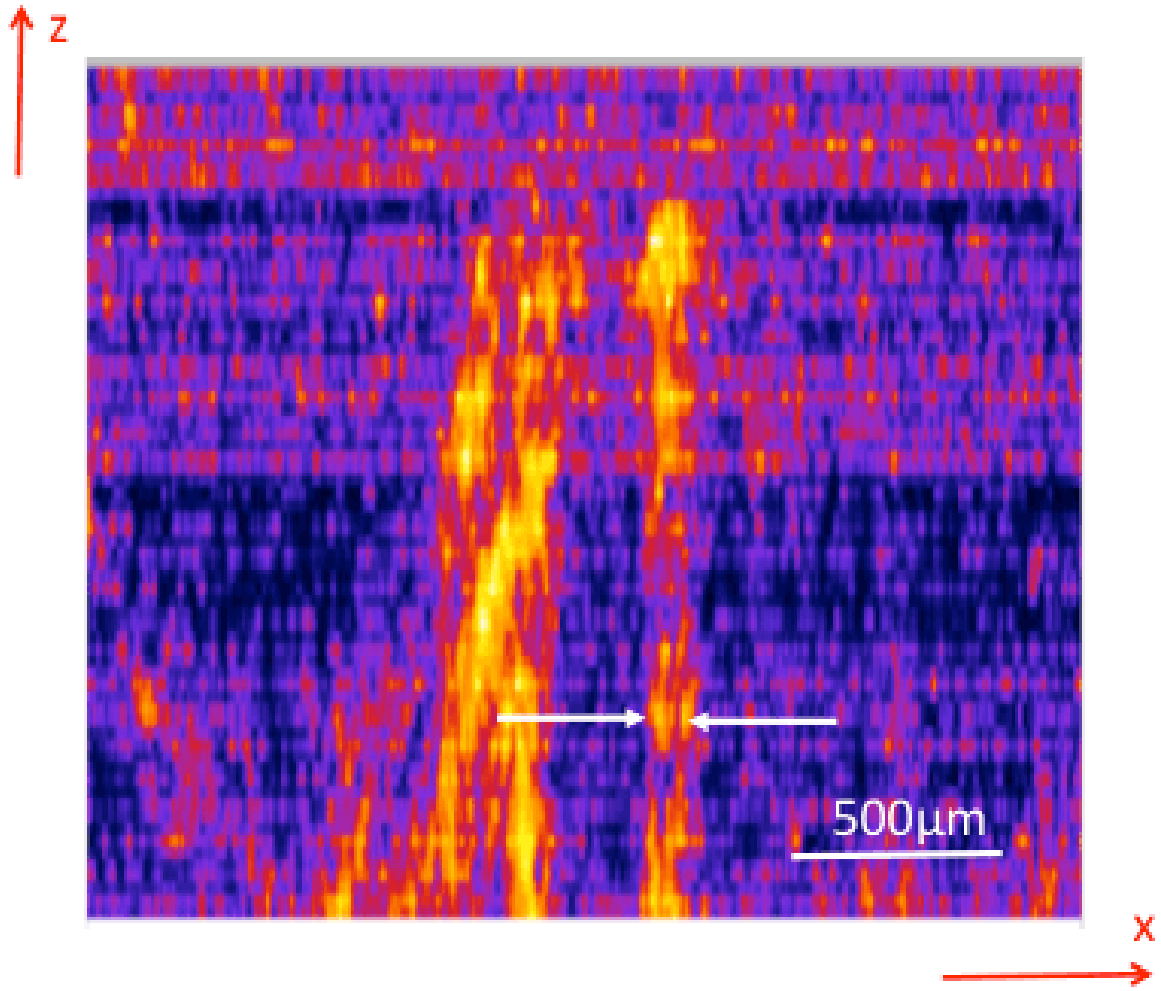

Figure 21 Carbon fiber network

3.3 Photoacoustic microscopy imaging using two-dimensional PZT scanner

A 2-D PZT scanner was used to replace the 1-D PZT scanner in the PAM system shown in Figure 14. As for the 2-D PZT scanner, the resonant fiber-tip deflection was 2.9 mm and the non-resonant fiber-tip deflection was 960 μm. Two function generators were used, and each one controlled one dimension of the 2-D PZT scanner to achieve 2-D scanning. Figure 22 shows the prototype 2-D scanner based PAM system.

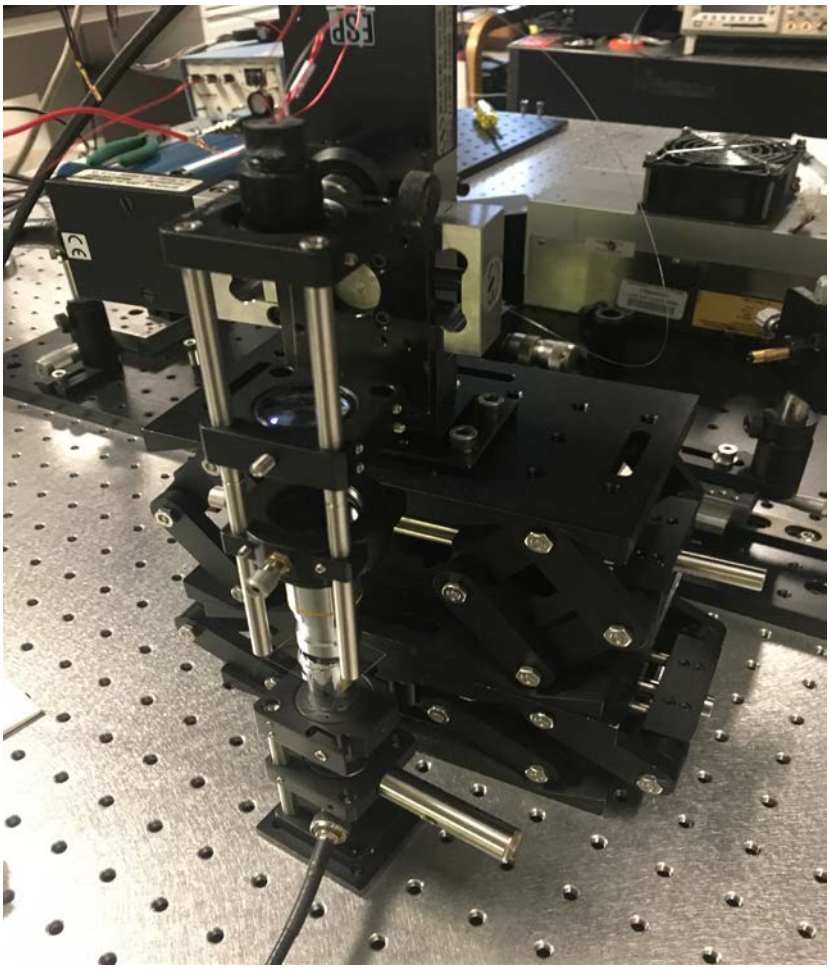

Figure 22 2-D PZT scanner based imaging system

A mechanical pencil lead was imaged using the system. The width of the pencil lead was 300 μm. It was placed in the direction that was parallel to the resonant scanning axis. Figure 23 shows the 3-D PAM image of the pencil lead. The axis x was the scanning axis of resonant PZT. The axis y was the scanning axis of non-resonant PZT. Since the scanning range of the non-resonant axis can reach 1 mm, the whole width of the pencil lead can be scanned. The resonant scanning speed was 64 Hz and the non-resonant scanning speed was 1 Hz. The laser repetition rate was 64 Hz and the pulse energy was 7.5 μJ. A B-scan of the pencil lead was also shown below the 3-D image (Figure 23).

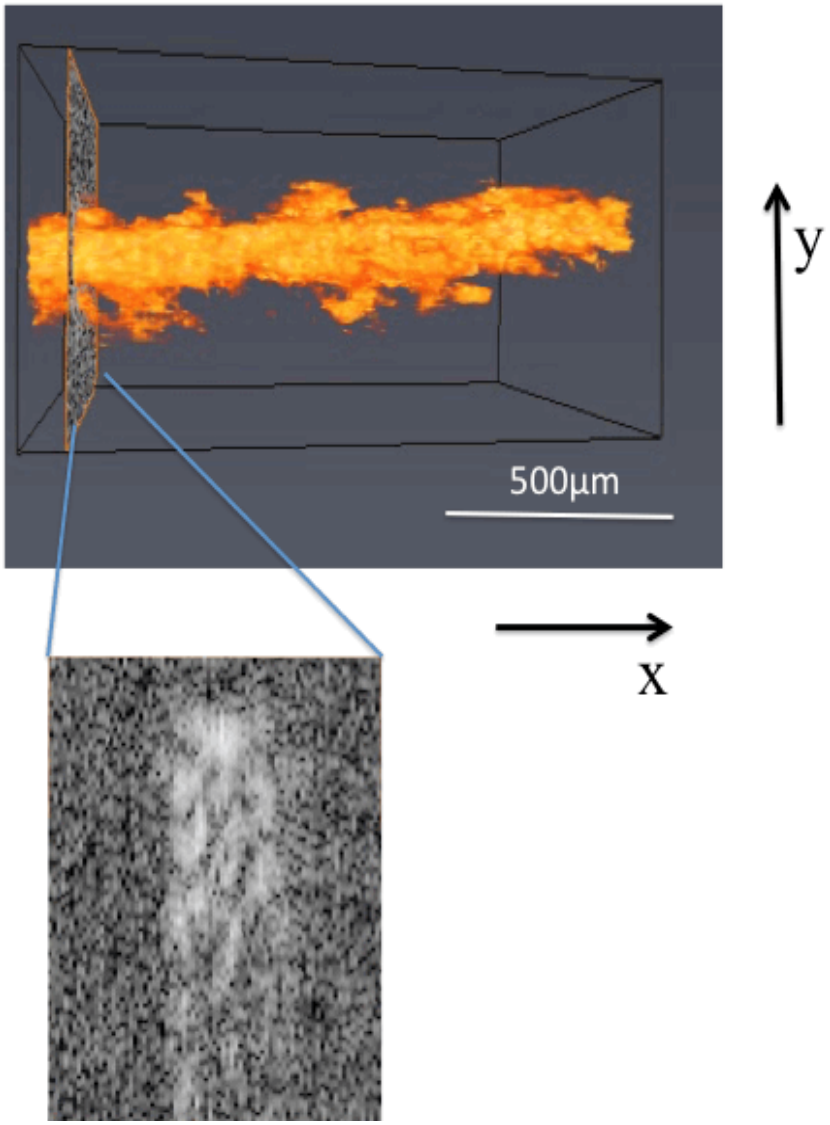

Figure 23 The 3-D PAM image of the mechanical pencil lead

Furthermore, a black plastic triangle was imaged using the system to test the 2-D scanning ability of the scanner (Figure 24). The resonant scanning speed was 64 Hz and the non-resonant scanning speed was 1 Hz. The laser repetition rate was 64 Hz and the pulse energy was 7.5 µJ. The axis y is the resonant scanning axis and the axis x is the non-resonant scanning axis. The maximum width of the triangle sample is 500 μm. And the height of the triangle is 800 μm.

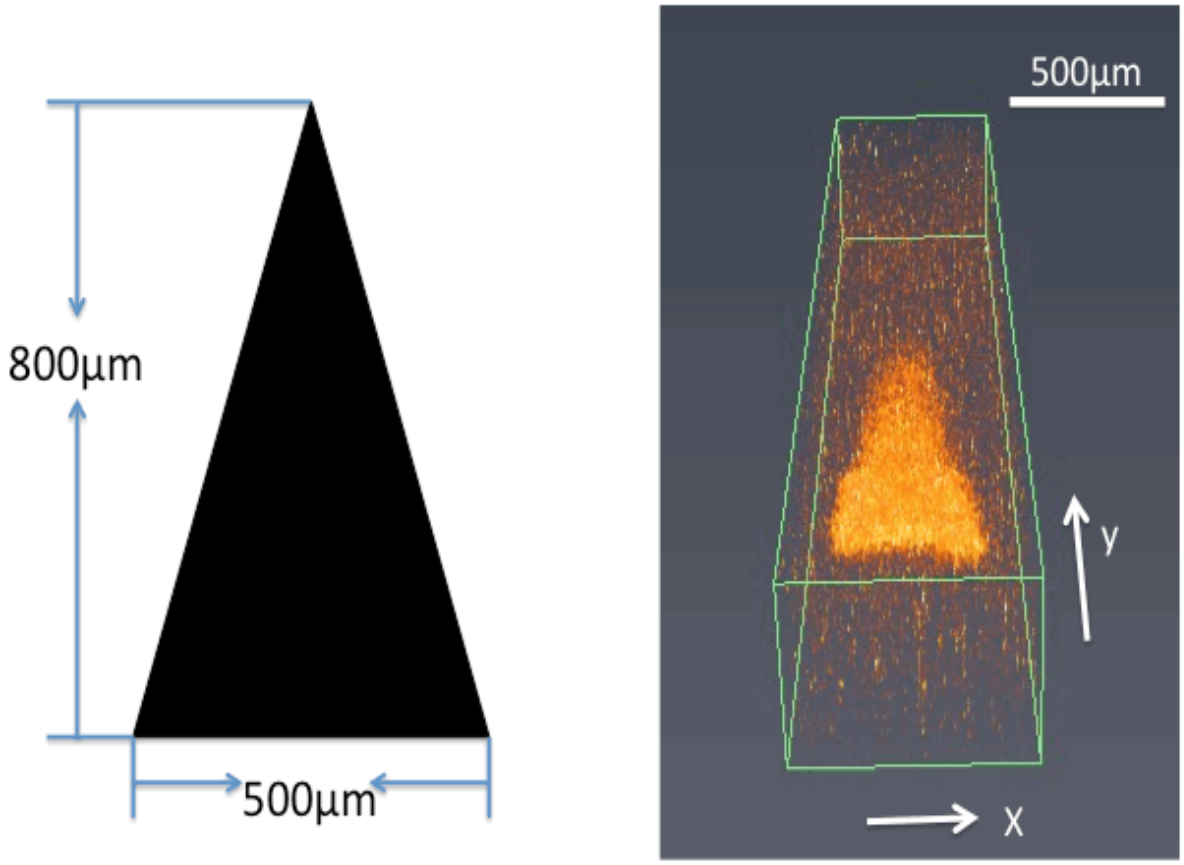

Figure 24 Black plastic triangle

The whole black triangle was imaged, under a sufficient FOV of the 2-D PZT scanner. And the well-imaged triangle proved that the 2-D PZT scanner has satisfied 2-D scanning ability. Compared to the linear stage-based scanner, the 2-D PZT scanner was simpler and more flexible. The only shortage of the 2-D PZT scanner is the limited scanning range. The maximum resonant fiber-tip deflection of the 2-D PZT scanner is 2.9 mm, while the maximum resonant fiber-tip deflection of the 1-D PZT scanner is 17.34 mm. The smaller fiber-tip deflection in the 2-D PZT scanner was caused by sticking the non-resonant PZT to the resonant PZT.

Furthermore, a very small non-resonant PZT was used to reduce the influence of the resonant PZT. The resonant fiber-tip deflection increased but the non-resonant fiber-tip deflection

decreased severely. Thus, the FOV of the 2-D PZT scanner cannot be the same size as the FOV of the 1-D PZT scanner. To increase the FOV, a multi-scanner scanning method shown in Figure 25 could be used in the future.

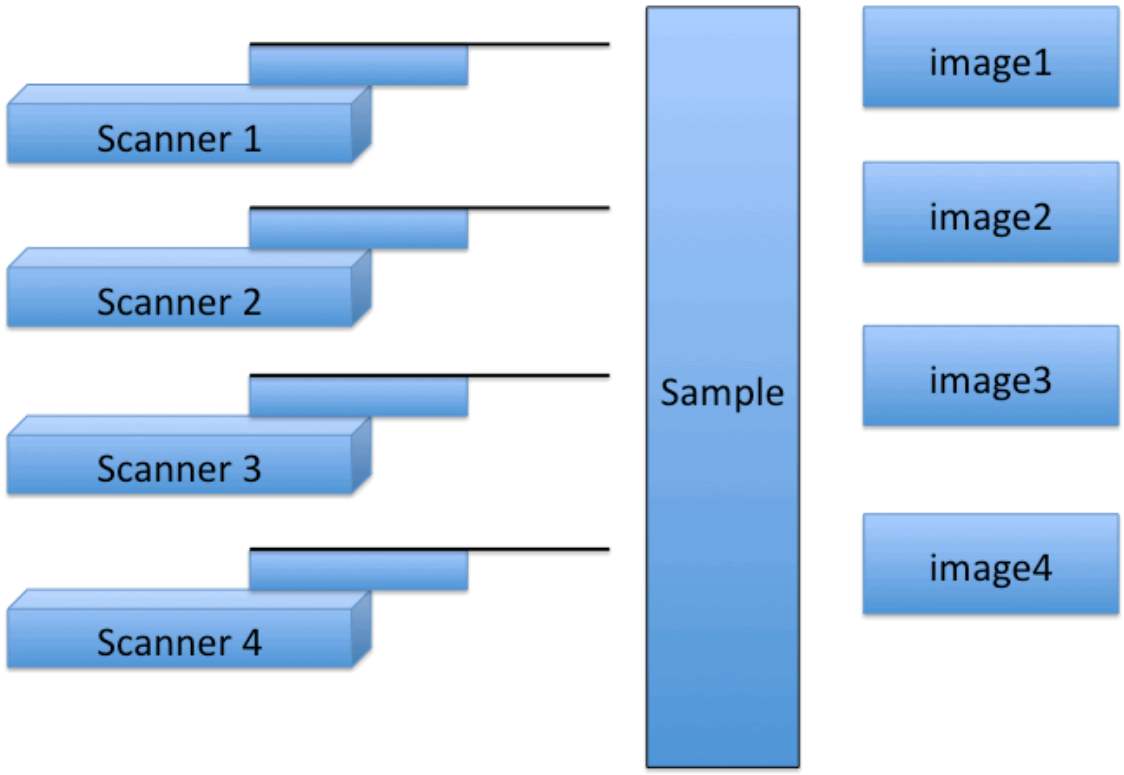

Figure 25 Multi-scanner based scanning method

Figure 25 indicates that when multi-scanners are working simultaneously, many small images can be obtained. Therefore, the FOV will be increased if these small images are combined into one large image.

III. Conclusion

The results of the experiments proved that the PAM system with PZT scanner has the ability to obtain the 2-D images. Furthermore, high resolution and sufficient FOV can be achieved using the PZT scanner based photoacoustic microscopy system. For the future, this type of photoacoustic microscopy system has a great potential to be used in broad clinical applications. Since the resonant scanning speed can achieve several thousand megahertz, this system can be integrated as a real-time ex vivo medical device for the detection of different diseases, such as skin cancer [12]. Moreover, many 2-D PZT scanners can be integrated into one device to solve the limited field-of-view problem. Furthermore, more efficient PZT with better performance may be produced in the future to improve the performance of the PZT-based PAM systems. In conclusion, it is expected that the PZT scanner-based imaging systems would be used in a wider range of biomedical engineering applications.

References

[1] Amos B. Lessons from the history of light microscopy[J]. Nature cell biology, 2000, 2(8): E151-E152.

[2] Wang L V, Wu H. Biomedical Optics, Principles and Imaging John Wiley & Sons[J]. Inc., Hoboken, New Jersey, 2007.

[3] Xu M, Wang L V. Photoacoustic imaging in biomedicine[J]. Review of scientific instruments, 2006, 77(4): 041101.

[4] Yao J, Wang L V. Photoacoustic microscopy[J]. Laser & photonics reviews, 2013, 7(5): 758-778.

[5] Zhang H F, Maslov K, Stoica G, et al. Functional photoacoustic microscopy for high-resolution and noninvasive in vivo imaging[J]. Nature biotechnology, 2006, 24(7): 848-851.

[6] Wang L V, Hu S. Photoacoustic tomography: in vivo imaging from organelles to organs[J]. Science, 2012, 335(6075): 1458-1462.

[7] Jaffe B. Piezoelectric ceramics[M]. Elsevier, 2012.

[8] Shrout T R, Zhang S J. Lead-free piezoelectric ceramics: Alternatives for PZT?[J]. Journal of Electroceramics, 2007, 19(1): 113-126.

[9] Rao B, Maslov K, Danielli A, et al. Real-time four-dimensional optical-resolution photoacoustic microscopy with Au nanoparticle-assisted subdiffraction-limit resolution[J]. Optics letters, 2011, 36(7): 1137-1139.

[10] Kinsler LE, Frey AR, Coppens AB, Sanders JV. Fundamentals of Acoustics (Wiley, New York), 3rd Ed., 1982.

[11] Rivera D R, Brown C M, Ouzounov D G, et al. Compact and flexible raster scanning multiphoton endoscope capable of imaging unstained tissue[J]. Proceedings of the National Academy of Sciences, 2011, 108(43): 17598-17603.

[12] Favazza C P, Cornelius L A, Wang L V. In vivo functional photoacoustic microscopy of cutaneous microvasculature in human skin[J]. Journal of biomedical optics, 2011, 16(2): 026004-026004-5.